Chemical Engineering Journal 165 (2010) 395–404

Contents lists available at ScienceDirect

Chemical Engineering Journal

journal homepage: www.elsevier.com/locate/cej

Modelling gas permeation through new microporous titanosilicate AM-3 membranes

Patrícia F. Lito [a], Chun F. Zhou [a], Ana S. Santiago [a], Alírio E. Rodrigues [b], João Rocha [a], Zhi Lin [a], Carlos M. Silva [a,*]

[a] CICECO, Department of Chemistry, University of Aveiro, 3810-193 Aveiro, Portugal
[b] LSRE, Departamento de Engenharia Química, Faculdade de Engenharia, Universidade do Porto, Rua Dr. Roberto Frias s/n, 4200-465 Porto, Portugal

ARTICLE INFO

Article history:
Received 13 April 2010
Received in revised form 14 July 2010
Accepted 15 July 2010

Keywords:
Membranes
Microporous titanosilicates
AM-3
Transport mechanism
Modelling

ABSTRACT

A new microporous titanosilicate AM-3 has been synthesized on alumina tubular support by seeded hydrothermal synthesis. The dynamic characterization has been carried out by permeation assays of single gases at fixed and programmed temperature, and for several transmembrane pressure drops. The mechanisms involved in the gas transport have been investigated, namely viscous, Knudsen, activated gaseous and surface diffusions. Results published for the first AM-3 membrane have been modelled as well in order to comprise all transport contributions occurring in porous media. The obtained results pointed out the existence of macro-, meso- and micro-defects. The representation of the experimental data was achieved successfully with absolute average relative deviations between 1.5% and 2.5%.

1. Introduction

Inorganic membranes generally exhibit a high thermal and chemical stability, and resistance to high transmembrane pressure differences which make them promising materials for gas separation applications [1]. Microporous titanosilicates are novel materials that may broaden the scope of application of classical zeolites. The structure of these materials consists of interlinked octahedral and tetrahedral frameworks. Similarly to zeolites, microporous titanosilicates exhibit a well-defined three-dimensional crystalline structure with the channel of molecular dimensions, being able to separate mixtures based on differences in affinity and sieving effect [2–5]. Moreover, they offer important benefits over classical zeolitic membranes, namely: (i) they are generally synthesized in the absence of organic templates, avoiding usual subsequent calcination treatments (at nearly 500 °C), which often cause irreversible defects and/or loss of active surface groups; (ii) they are usually prepared under moderate pH conditions, reducing chemical attack to the support; (iii) they exhibit novel possibilities of isomorphous framework substitution, allowing for fine-tuning catalytic and adsorption properties; and (iv) generally, they have strong alkalinity, complementing the acid properties of classic zeolites [6].

AM-3 (Aveiro–Manchester number 3) is a synthetic microporous titanosilicate analogue of mineral penkvilksite-2*O*, with an ideal formula $Na_2TiSi_4O_{11}{\cdot}2H_2O$ [3]. Its structure consists of SiO_4 tetrahedra chains connected by individual TiO_6 octahedra forming a three-dimensional framework with 6-ring channels [7]. In a previous work it was shown that AM materials do not adsorb any significant amount of nitrogen but do adsorb water in relatively large quantities [3]. In addition, AM-3 was demonstrated to be stable up to ca. 600 °C, loosing water and rehydrating reversibly after being kept in air for a few hours at room temperature. A detailed morphological characterization of AM-3 was first reported by Lin et al. [3] and later by Rocha and Anderson [2].

The molecular sieving action of microporous zeolites, together with their large specific surface areas and controlled host–sorbate interactions, are important motivations in zeolitic membranes. In particular for small gases separation, narrow pore materials are crucial for an effective molecular sieving effect. For instance, hydrogen is nowadays considered an alternative clean fuel for future sustainable energy economy. Zeolite membranes offer excellent thermal and hydrothermal stability, but the pore size of most applied materials is generally not sufficient narrow for highly selective H_2 separations. Titanosilicate membranes may become especially competitive for industrial applications due to their small pores, promoting an effective size-exclusion separation. The small dimensions of AM-3 pores could anticipate the potential of

* Corresponding author at: Department of Chemistry, University of Aveiro, Campus Universitário de Santiago, 3810-193 Aveiro, Portugal. Tel.: +351 234 401 549; fax: +351 234 370 084.
E-mail address: carlos.manuel@ua.pt (C.M. Silva).

1385-8947/$ – see front matter © 2010 Elsevier B.V. All rights reserved.
doi:10.1016/j.cej.2010.07.036

Nomenclature

AARD	Average absolute relative deviation (%)
B	Mobility of diffusing gas (mol m^2 J^{-1} s^{-1})
b	Equilibrium adsorption constant (Pa^{-1})
D	Self-diffusion coefficient (m^2 s^{-1})
Đ	Maxwell–Stefan (MS) diffusivity (m^2 s^{-1})
d_p	Pore diameter (m)
E_a	Activation energy (J mol^{-1})
g	Geometrical factor
ΔH_{ads}	Enthalpy of adsorption (J mol^{-1})
J	Molar diffusion flux (mol m^{-2} s^{-1})
l_d	Diffusion length (m)
P	Total pressure (Pa)
Q_{st}	Isosteric adsorption energy (J mol^{-1})
q	Molar concentration of adsorbed species in the solid (mol kg^{-1})
$\Re$	Universal gas constant (J mol^{-1} K^{-1})
T	Temperature (K)
Z	Number of adjacent active sites
z	Distance coordinate (m)

Greek letters

δ	Membrane thickness (m)
ε	Porosity
τ	Tortuosity
Γ	Thermodynamic factor
θ	Fractional occupancy
λ	Mean free path (m)
μ	Chemical potential (J mol^{-1})
ν	Jump frequency (s^{-1})
η	Viscosity (Pa s)
Π	Permeance (mol m^{-2} s^{-1} Pa^{-1})
ρ_p	Density (kg m^{-3})

Subscripts

f	Feed side
g	Gaseous
kn	Knudsen
p	Permeate side
s	Surface
v	Viscous

Superscripts

o	Reference condition

these membranes for real applications concerning purification of hydrogen-containing streams.

The understanding of mass transport mechanisms is essential for an accurate modelling of the permeances. Modelling is fundamental for interpretation of experimental data and as a predictive tool. Prediction and correlation of permeation requires knowledge on diffusion, adsorption and structure parameters, which may be determined by experimental methods and adequate modelling of transport phenomena.

The transport mechanisms involved in porous media are primarily related with pore diameter, d_p. Accordingly, viscous flow dominates in macropores ($d_p > 50$ nm), where the fluid flows as a whole under a pressure gradient. In mesopores and micropores ($2 < d_p < 50$ nm and $d_p < 2$ nm, respectively), collisions between molecules and pore surface are fundamental. When the mean free path, λ, (i.e. the average distance traversed by a molecule between collisions) is comparable or larger than the pore diameter, transport falls in the Knudsen regime. In small micropores, pore size approaches molecular dimensions and the molecules are not as free as in Knudsen diffusion, where the effect of the potential field of the solid surface is minimal [8]. In this case, commonly described as configurational diffusion, molecules may never completely escape from the force field of the surface [9] and diffusion becomes an activated process. Based on the mode of translational motion of molecules inside the pores, two distinct mechanisms may be distinguished here: molecules may retain their gaseous state (gas translational or activated gaseous diffusion) or lose their gaseous entity due to strong interaction with the solid framework and move as an adsorbed phase [9].

Several approaches have been proposed in literature to describe surface diffusion [8,10,11], including the *hopping model*, by which molecules move over the surface by hopping between adjacent adsorption sites (minima in the potential energy field of the pore) [9,12–14], the *hydrodynamic model*, in which adsorbed molecules are considered as a fluid film, which merely slide along the surface [12,15], and the *random walk model*, based on the two-dimensional form of Fick's first law. Nonetheless, the hopping model is the most frequently adopted for modelling surface diffusion in micropores [9,13,16–22], being adopted as well in this paper.

Similarly to the surface diffusion, the activated transport of gaseous molecules inside the pore may be assumed to occur by a sequence of jumps from site to site, restricted by the energy barrier imposed by the surface. Several authors reported the activated gaseous diffusion as an activated process analogous to a Knudsen mechanism, denoting it by activated Knudsen diffusion [8,10,23,24]. However, Burggraaf and Cot [8] presented a slightly different concept to describe this mechanism. In their description, molecules are assumed to move freely between adsorption sites, involving an activated sub-step and a Knudsen diffusion step. This situation is reported for a ratio between pore diameter and kinetic molecular diameter around two. Moreover, the configurational diffusion regime is reached with decreasing pore size, where the remaining gaseous state within the pore is assumed to be vanished and only surface diffusion may occur.

In this work a new microporous titanosilicate AM-3 membrane (hereafter denoted by AM-3-1) was synthesized and characterized by single gas permeation measurements. The permeation data obtained were modelled based on the several transport mechanisms involved in porous media, which are presented and discussed in the following section. Data for a distinct AM-3 membrane (henceforth labelled AM-3-2) were also modelled as well in order to complement the analysis of these new titanosilicate membranes.

2. Modelling gas transport mechanisms

2.1. Viscous flow

In macropores the molar flux, J_v, under a pressure gradient may be described by a Hagen–Poiseuille type-law:

$$J_v = -\frac{\varepsilon}{\tau}\frac{d_p^2}{32\eta}\frac{P}{\Re T}\frac{dP}{dz} \quad (1)$$

where η is the gas viscosity, P and T are the total pressure and temperature, respectively, $\Re$ is the universal gas constant, and z is distance coordinate. The factor ε/τ is introduced in the flux equation to account for geometrical effects of the porous structure, being ε and τ the porosity and tortuosity, respectively. At steady state, the permeance through a porous membrane may be obtained after integration of Eq. (1) over the membrane thickness, δ:

$$\Pi_v \equiv \frac{J_v}{\Delta P} = \frac{\varepsilon d_p^2}{32\eta\tau}\frac{P_m}{\delta \Re T} \quad (2)$$

where P_m is the arithmetic mean pressure between two sides of the membrane.

2.2. Knudsen diffusion

Knudsen diffusion prevails in mesopores, where the mean free path of diffusing species is close to the pore diameter [25]. Under this regime, molecule-pore wall collisions are important, being responsible for diffusion. The Knudsen diffusivity, D_{Kn}, may be expressed as [9]:

$$D_{Kn} = \frac{d_p}{3}\left(\frac{8\Re T}{\pi M}\right)^{0.5} \tag{3}$$

where M is the molecular weight of the diffusing gas; the geometric factor 1/3 is introduced since only those molecules moving in the direction under consideration must be taken into account. The expression for Knudsen diffusion flux, J_{Kn}, may be obtained by combining Eq. (3) with Fick's first law [26,27]:

$$J_{Kn} = -\frac{\varepsilon d_p}{3\tau}\left(\frac{8}{\pi\Re TM}\right)^{0.5}\frac{dP}{dz} \tag{4}$$

The Knudsen permeance through a porous membrane may be found after integration of Eq. (4) over the membrane thickness:

$$\Pi_{Kn} \equiv \frac{J_{Kn}}{\Delta P} = \frac{\varepsilon d_p}{3\tau\delta}\left(\frac{8}{\pi M\Re T}\right)^{0.5} \tag{5}$$

2.3. Diffusion in micropores

Mass transport of single gases is generally described by the Fick's first law, where a concentration gradient is assumed to be the driving force. However, the true driving force for diffusion is believed to be the chemical potential gradient [28], which is most relevant in microporous systems. Accordingly, the permeation flux of a single gas in micropores (in the z-direction), in isothermal conditions, should be:

$$J = -B\rho q\frac{\partial\mu}{\partial z} \tag{6}$$

where B is the mobility of diffusing gas, q is its molar concentration in the particle, ρ is the particle density, and μ is the chemical potential. Assuming the gas phase as ideal, the following relationship may be obtained:

$$J = -\rho q\text{Đ}\frac{d\ln P}{dz} \tag{7}$$

where $\text{Đ} = B\Re T$ is a corrected diffusion coefficient equivalent to a Maxwell–Stefan diffusivity [13,18,29]. Similarly to the Maxwell–Stefan formulation, a thermodynamic factor may be defined as $\Gamma = \partial\ln P/\partial\ln q$, and the expression for permeation may be written as:

$$J = -\rho\text{Đ}\Gamma\frac{dq}{dz} \tag{8}$$

As may be easily observed, Fick and corrected diffusivities are related by the thermodynamic factor as $D = \text{Đ}\,\Gamma$.

2.4. Activated gaseous diffusion

The diffusivity of gaseous molecules may be given by [9]:

$$D_g = \frac{1}{Z}l_d\left(\frac{8\Re T}{\pi M}\right)^{0.5}\exp\left(\frac{-E_{a,g}}{\Re T}\right) \tag{9}$$

where l_d is the distance between two adjacent sites of low energy, $1/Z$ is the probability of a molecule moving in the direction under consideration, being Z the number of adjacent sites, and $E_{a,g}$, is the energy required for molecules to surmount the attractive constraints imposed by the pore structure. Since there is no formal adsorption, the flux may be expressed in terms of pressure. Hence, one may obtain, after integration over membrane thickness:

$$\Pi_g \equiv \frac{J_g}{\Delta P} = \frac{l_d}{Z\delta}\left(\frac{8}{\pi M\Re T}\right)^{0.5}\exp\left(\frac{-E_{a,g}}{\Re T}\right) \tag{10}$$

Eq. (10) shows an exponential dependence of gas permeance on the temperature, differently from that of the Knudsen model.

2.5. Surface diffusion

For surface diffusion of adsorbed molecules, Fick diffusivity may be expressed as [9]:

$$D_s(q) = \frac{1}{Z}{l_d}^2\nu(q)\exp\left(\frac{-E_{a,s}}{\Re T}\right) = D_s^0(q)\exp\left(\frac{-E_{a,s}}{\Re T}\right) \tag{11}$$

being $E_{a,s}$ the activation energy for surface diffusion and $\nu(q)$ the jump frequency. According to the relation between Fick and corrected diffusivities, it follows:

$$D_s(q) = \text{Đ}_s\Gamma = \text{Đ}_s^0\Gamma\exp\left(\frac{-E_{a,s}}{\Re T}\right) \tag{12}$$

In order to determine the thermodynamic factor, Γ, the isotherm must be known. The adsorption of gas molecules in microporous membranes occurs frequently in monolayer, being accurately described by the Langmuir isotherm. In this case, the thermodynamic factor reduces to:

$$\Gamma = \frac{1}{1-\theta} \tag{13}$$

The permeance of adsorbed molecules in micropores may be then obtained, after integration over the membrane thickness:

$$\Pi_s \equiv \frac{J_s}{\Delta P} = \frac{\rho}{\delta}q_{sat}\text{Đ}_s^0\exp\left(\frac{-E_{a,s}}{\Re T}\right)\ln\left(\frac{1-\theta_p}{1-\theta_f}\right)\frac{1}{P_f - P_p} \tag{14}$$

where subscripts f and p identify feed and permeate conditions, respectively. At low pressures the Henry's regime for adsorption is frequently valid, i.e.:

$$q = KP \tag{15}$$

where K is the Henry's constant. The dependence of K on temperature may be also given by a van't Hoff-type relation:

$$K = K_0\exp\left(\frac{Q_{st}}{\Re T}\right) \cong K_0\exp\left(\frac{-\Delta H_{ads}}{\Re T}\right) \tag{16}$$

Accordingly, the permeance under the Henry's regime is given by:

$$\Pi_s \equiv \frac{J_s}{\Delta P} = \frac{\rho}{\delta}D_s^0K_0\exp\left(\frac{\Delta H_{ads} - E_{a,s}}{\Re T}\right) \tag{17}$$

2.6. Gas permeation through microporous membranes

It is generally found that both surface and activated gaseous diffusion mechanisms contribute to the overall mass transport through microporous membranes. The individual contributions to the total permeation depend mainly on the adsorption properties of the system, as well as on the conditions of temperature and pressure [30,31,32]. Moreover, in real membrane systems, Knudsen diffusion and/or viscous flow may be expected to contribute to the total permeation flux as well, owing to the presence of defects in the crystalline structure.

Assuming the permeances from different diffusion mechanisms are additive, the total permeance through microporous membranes may be written as follows:

$$\Pi_{total} = \Pi_{defects} + \Pi_{micropores} = \Pi_v + \Pi_{Kn} + \Pi_s + \Pi_g \tag{18}$$

It is worth noting that the effect of the support must be taken into account in the calculation of the effective Π_{total}, since only

a fraction of the total area is available for permeation. Thus, Eq. (18) must be multiplied by a support geometric factor, which is commonly associated to its porosity.

The transport mechanism controlling the permeation process may be discriminated from the permeance–temperature behaviour, in agreement with the previous discussion. For instance, diffusion of non-adsorbable gases in micropores is expected to increase monotonically with temperature. However, a minimum in the permeance is frequently found at low temperatures, which can be ascribed to the presence of defects, since permeation flux resulting from both viscous and Knudsen mechanisms decreases with increasing temperature. The transport of strongly adsorbable molecules at low or moderate temperatures is dominated by surface diffusion, while activated gaseous diffusion may prevail at high temperatures [33–35]. In this case, a maximum followed by a minimum in the permeance should be anticipated [16,36–38]. At low temperatures, permeance increases because the diffusivity of adsorbed molecules is enhanced by temperature, even though the surface coverage simultaneously decreases; at a given temperature, the decrease in the adsorbed concentration becomes the determining factor, so that the overall permeance will start to decrease. At higher temperatures, adsorption could be negligible and permeance would be expected to exponentially increase, given the activated nature of diffusion through micropores [39]. Once more a minimum in the permeance is commonly observed at lower temperatures, which may be attributed to an additional contribution of viscous and/or Knudsen mechanisms.

3. Material and methods

3.1. Membrane synthesis and characterization

AM-3 membrane (denoted by AM-3-1) has been prepared on commercial tubular symmetric α-alumina (Inopor) support by subjecting the seeded support to a secondary growth step, which was performed in Teflon-lined autoclaves at 230 °C under autogenous pressure without rotation. The α-alumina support used in this experiment has a pore size of 3.0 μm and the thickness of ca. 1.5 mm. Before the hydrothermal synthesis, the support was seeded by rubbing AM-3 seeds. AM-3 seed was made according to our previous work [3] and the XRD pattern and SEM image of AM-3 seeds were shown in Fig. 1a. The inner side of the 8 cm long tube was not seeded, reducing the crystal growth in this region. The seeded support was placed vertically in the bottom of a Teflon-lined autoclave with Teflon holder where the growth (synthesis) gel was poured. Sodium silicate solution (27 wt.% SiO_2, 8 wt.% Na_2O, Merck) and titanium trichloride solution (15 wt.% $TiCl_3$, 10 wt.% HCl, Merck) are used as Si and Ti sources. The precursor for AM-3 membrane synthesis was prepared as follows. 32.51 g of sodium silicate solution was diluted in 15.36 g of distilled water. Then, 6.40 g of sodium hydroxide (Merck), 3.74 g of sodium chloride (Panreac) and 2.86 g of potassium chloride (Merck) were added. Finally, 29.50 g of titanium trichloride solution was added with thorough stirring and homogenised for more than 30 min. This process results in a viscous mixture. This mixture, with a molar composition 5.4 Na_2O:0.6 K_2O:5.1 SiO_2:1.0 TiO_2:113 H_2O, was treated at 230 °C for 48–96 h. The autoclave was cooled down by flowing water and the sample was washed with distilled water. Finally, the AM-3 membrane was treated with 2 wt.% NaCl solution in Teflon-lined autoclave at 150 °C for 5 h and washed with distilled water again. This process is used to remove undesired residues in the pores and at the same time to keep AM-3 in Na-form. The membrane can be reproduced with similar morphological quality.

The phase was identified by X-ray diffraction at room temperature in a step-scan regime on an X'Pert MPD Philips diffractometer using Cu Kα radiation in the 2θ range 5–50°. Scanning electron microscopy (SEM) images were recorded on a Hitachi S-4100 microscope.

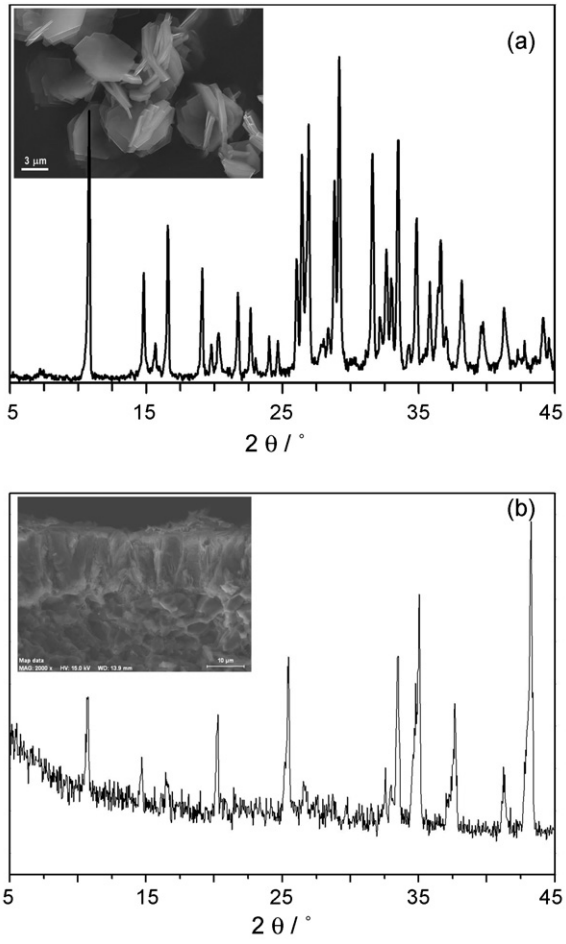

Fig. 1. X-ray diffraction patterns and scanning electron microscopy images of (a) AM-3 seed and (b) AM-3-1 membrane.

3.2. Permeance measurements

Thermal pre-treatment. In order to remove adsorbed water and eventually other compounds, a heating and cooling cycle was always carried out up to ca. 200 °C. During this pre-treatment, a continuous He flow (20 cm^3(PTN)/min) was imposed through the membrane.

Measurement of nitrogen permeance at room temperature. This experiment was firstly carried out to detect rough defects in the membrane, which has been assumed for permeances higher than 10^{-6} mol m^{-2} s Pa, since over-enhanced values denunciate the presence of macro- or meso-defects. The membrane was placed inside a stainless-steel module at constant temperature (25 °C) and sealed with viton o-rings in order to avoid the mixture of permeate and feed streams. The retentate side was blocked during experiments (dead-end mode) to promote total permeation of nitrogen. The feed flow rate was fixed with a mass flow controller (MFC), the permeate side was kept at atmospheric pressure, and the resulting transmembrane pressure drop was registered. The stationary state was detected when the mass flow meter (MFM) located at permeate outlet confirmed the MFC display. Experiments were repeated for different feed flows, between 5 and 20 cm^3(PTN)/min, and the permeance obtained by the slope of the permeation flux *versus* ΔP plot. The permeable area of the membrane was 1.7×10^{-3} m^2.

Permeation of single gases at programmed temperature (PPT). Studied gases: He, H_2, N_2, and CO_2. The membrane module was placed inside the oven, the feed flow rate was fixed with the MFC, the permeate side was kept at atmospheric pressure, and ΔP was controlled by a backpressure regulator located at retentate outlet. Experiments were conducted between 25 and 120 °C, at a fixed heating rate of 1 °C min^{-1}, for transmembrane pressure drops of 100 and 200 kPa. Permeances were computed by the ratio between the measured permeation fluxes and ΔP. It is important to refer that no reproducibility problems were experienced during the permeation measurements.

4. Results

4.1. Membrane and crystal characterization

Fig. 1a shows the XRD pattern and SEM image of AM-3 seeds. This figure points out the intergrowth of high crystalline AM-3 plates with the average thickness of 500 nm. XRD and SEM characterizations confirmed the formation of an AM-3 membrane (Fig. 1b). Well crystalline and pure AM-3 is the only phase present on the support surface, although some peaks corresponding to the α-alumina support were also observed. SEM images displayed a typical crystal shape of AM-3 phase. Details may be found in Refs. [3,40].

A thermogravimetry analysis of AM-3 crystals was carried out in air between 25 and 170 °C at 2 °C min^{-1}. The obtained results, shown in Fig. 2, reveal that the weight loss and gain were relatively fast, indicating rapid moisture adsorption and desorption kinetics. Such finding evidences the absence of important water diffusion limitations, which ensures that the heating and cooling cycles performed before the permeation tests are effective.

4.2. Single gas permeation

The synthesized AM-3-1 membrane was firstly analysed by measuring N_2 permeance at room temperature, in order to investigate the existence of rough defects in AM-3 layer. The kinetic diameter of N_2 (0.346 nm) is larger than AM-3 pore diameter (0.3 nm), thus ideally no permeance should be detected at all. However, a perfect microporous membrane is difficult to achieve and macro-, meso- or even micro-defects may be always present in real systems. The permeance obtained, 3.14×10^{-8} mol m^{-2} s Pa, is inferior to the reference range taken for small gases permeances through microporous membranes (10^{-6} mol m^{-2} s Pa), which point out the absence of a considerable amount of rough deficiencies.

After that, the permeances of He, H_2, N_2, and CO_2 were measured along with temperature. Fig. 3 shows the PPT results for these

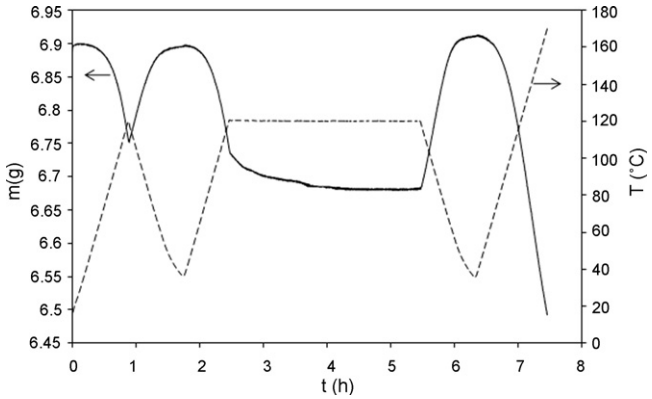

Fig. 2. Thermogravimetry analysis of AM-3 crystals.

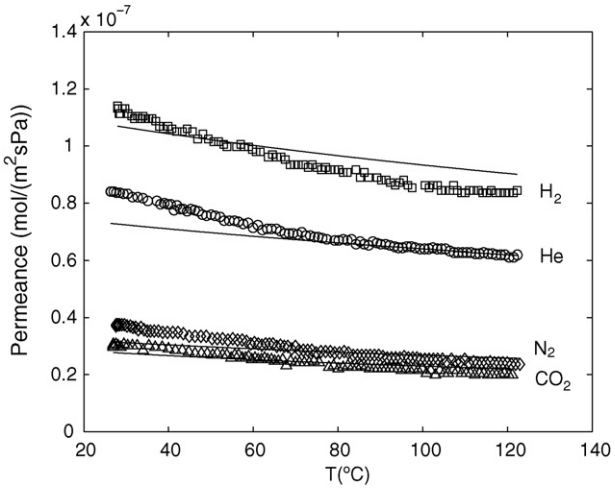

Fig. 3. Permeances of He, H_2, N_2 and CO_2 measured at programmed temperature in the AM-3-1 membrane for ΔP = 1 bar; experimental results (symbols) and modelling (lines).

gases, measured under the same transmembrane pressure drop of 1 bar. As may be observed, CO_2 and N_2 show similar permeances of 0.2–0.4 × 10^{-7} mol m^{-2} s Pa, which are significantly lower than those of He and H_2 (0.7–1.2 × 10^{-7} mol m^{-2} s Pa). It should be noted that the permeation of bulkier N_2 and CO_2 molecules may be only attributed to the transport through defects larger than the AM-3 pores, since their kinetic diameters (0.364 and 0.33 nm, respectively) are larger than the AM-3 pore size (0.3 nm). On the other hand, since H_2 and He are smaller than the pore diameter, one could expect they add an activated diffusion contribution. However, in membranes with significant defect density the influence of the defects may overcome the activated contribution in the micropores. Therefore, the descending pattern of this membrane may be considered a reliable indicator of the presence of defects.

Fig. 4 compares the permeance of He, H_2, and N_2 obtained for two distinct transmembrane pressure drops: 1 and 2 bar; results for CO_2 are not since they practically overlapped those of N_2. It is clear that ΔP has only a mild effect on the permeance, especially for He and H_2. However, an increase of the permeance with pressure was found for all the gases, corroborating the contribution of viscous flow to the total permeation. It is important to note that He and H_2 diffusion is less dependent on the pressure, since their transport

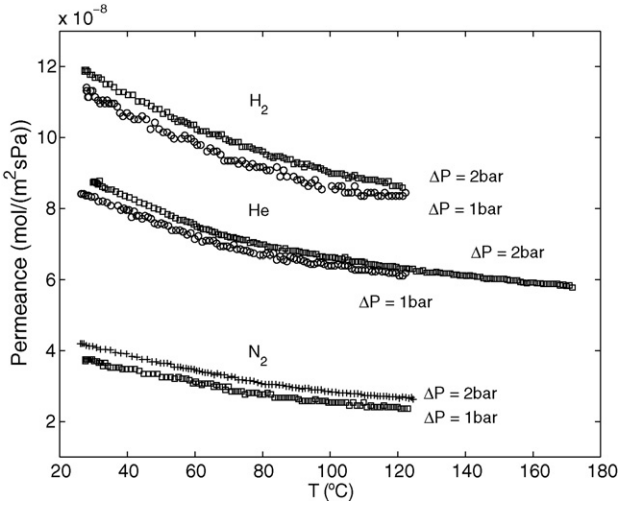

Fig. 4. Permeances measured at programmed temperature in the AM-3-1 membrane under ΔP = 1 and 2 bar for He, H_2, and N_2.

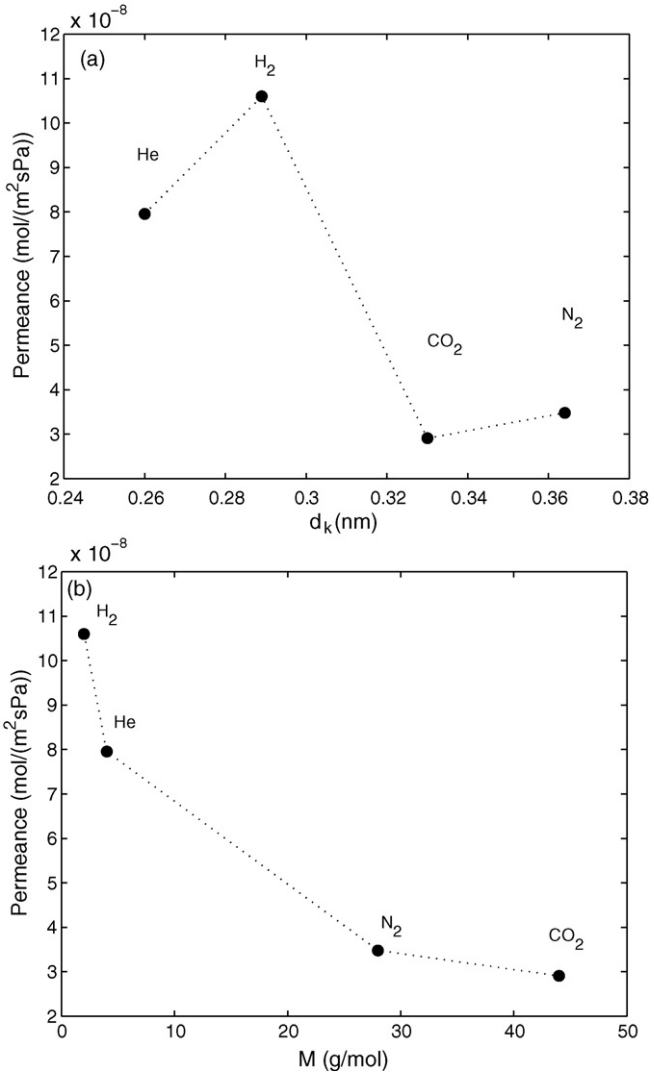

Fig. 5. Dependence of He, H_2, N_2 and CO_2 permeances at 40 °C and ΔP = 1 bar in the AM-3-1 membrane on (a) gas molecular diameter and (b) molecular weights data.

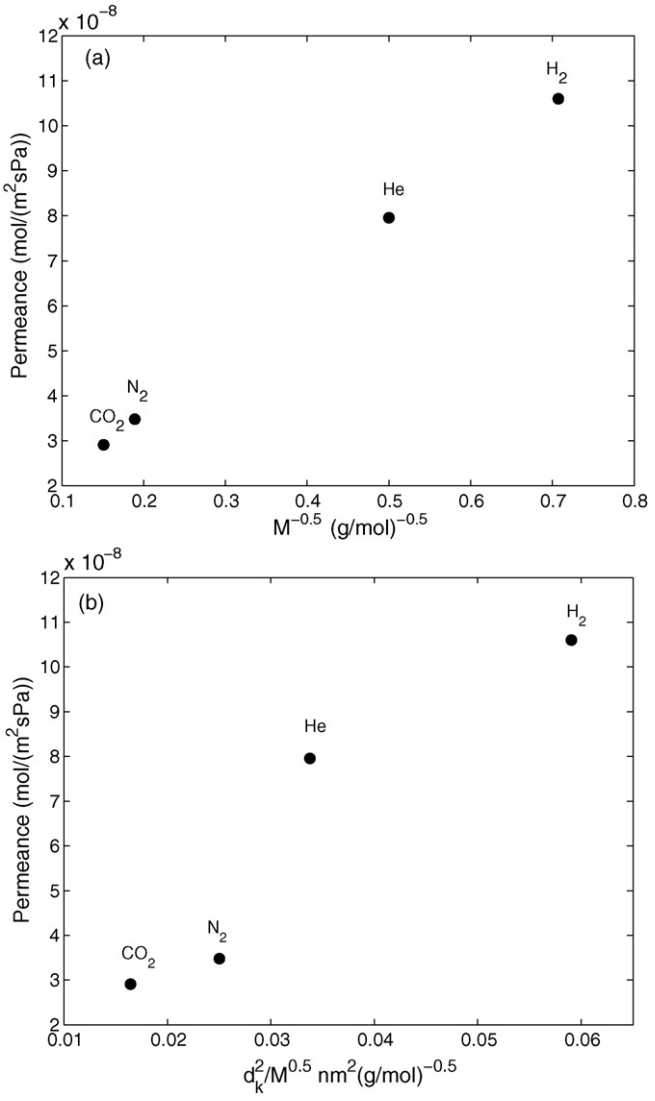

Fig. 6. Permeances of He, H_2, N_2, and CO_2 at 40 °C and ΔP = 1 bar in AM-3-1 membrane as function of (a) the inverse of the square root of their molecular weight and (b) the ratio between the square of kinetic diameter and the inverse of the square root of their molecular weight.

may occur through micropores and defects simultaneously, while N_2 and CO_2 diffuse uniquely through defects given their kinetic diameters larger than AM-3 pore size. Accordingly, the contribution from viscous flow is expected to be more important for N_2 and CO_2. In particular, Fig. 4 presents two almost overlapped permeation curves for He at ΔP = 2 bar, one measured up to 120 °C, and the other up to 170 °C. The results for the second PPT experiment are consistent with those after 120 °C, and reveal the predominance of gas transport through macro- and/or meso-defects even for higher temperatures. In addition, the membrane is found to be stable during repeated heating and cooling cycles in this temperature range.

The relationships between the permeances and the kinetic diameters and molecular weights of the diffusing gases are presented in Fig. 5. The figure shows a permeance dependence on both parameters. Moreover, as previously discussed, a pronounced permeance decline may be observed for gases with kinetic diameter superior to the AM-3 pore size (CO_2 and N_2 in contrast to He and H_2), reporting at least some molecular sieving effect (see Fig. 5a). Observed results also point out a clear trend of decreasing permeance with increasing molecular weight, following the typical behaviour of Knudsen diffusion (see Fig. 5b and Eq. (5)). The dominance of the Knudsen mechanism can be further verified in Fig. 6, where the permeance of the four studied gases shows a linear trend with the inverse of the square root of the molecular weight (see Fig. 6a), as expected for this transport mechanism (according to Eq. (5)). Concerning the viscous flow mechanism, its dependence on gas viscosity implies a dependence on both kinetic diameter and molecular weight. Following, for instance, the method of Chung et al. [41] for estimating gas viscosity, based on the theory of Chapman and Enskog, such dependence corresponds to $\eta \propto M^{0.5}/d_k^2$. It is clear from Fig. 6b that our permeances follow this relation, indicating as well some contribution from viscous flow.

According to the previous results, it may be concluded that gas transport through this AM-3-1 membrane is clearly dominated by both Knudsen and viscous flow mechanisms.

Experimental data for single gas permeation were modelled based on the transport mechanisms described previously in the modelling section. Transport through macro- and meso-defects was described by both Knudsen and viscous flow, while micropore diffusion was assumed to occur by the activated gaseous mechanism. Previous studies [3] have revealed that N_2 is practically non-adsorbed on AM-3. Since all permeation results do not evidence the contribution of surface diffusion, (i.e. the presence of

Table 1
Model parameters obtained for AM-3-1 and AM-3-2 membranes.

	$g_{sup}\frac{\varepsilon d_p^2}{32\tau\delta\Re}$ (m mol K/J) Eq. (2)	$g_{sup}\frac{\varepsilon d_p}{3\tau\delta}\left(\frac{8}{\pi\Re}\right)^{0.5}$ (mol K/J)$^{0.5}$ Eq. (5)	$g_{sup}\frac{l_d}{Z\delta}\left(\frac{8}{\pi\Re}\right)^{0.5}$ (mol K/J)$^{0.5}$ Eq. (10)	$E_{a,g}$ (kJ/mol) Eq. (10)				
				H_2	He	N_2	CO_2	O_2
AM-3-1	2.309×10^{-16}	7.244×10^{-8}	1.719×10^{-11} (N_2 and CO_2) 2.148×10^{-10} (H_2 and He)	13.3	11.0	1.7	4.0	–
AM-3-2	1.285×10^{-14}	3.869×10^{-7}	4.916×10^{-6} (N_2, CO_2, O_2) 1.769×10^{-5} (H_2)	10.0	–	3.0	4.6	5.5

a minimum followed by a maximum in the $\Pi - T$ curve), for the remaining gases it was not taken into account.

Eq. (18) was adopted to fit the experimental data of Fig. 3, by taking $\Pi_s = 0$ as aforementioned. A geometric factor, g_{sup}, was included in order to take the support effect into account. The membrane geometrical parameters for Knudsen and viscous flow mechanisms were considered equal for all gases, since they depend uniquely on membrane features. In contrast, for activated diffusion one distinct constant accounting for geometrical parameters was fixed for molecules capable of permeating AM-3 pores (H_2 and He) and another one for molecules larger than AM-3 pore diameter (N_2 and CO_2). This distinction is due to the fact that N_2 and CO_2, and H_2 and He diffuse through different microporous pathways: the first molecules through larger intercrystalline micropores, whereas H_2 and He permeate also AM-3 structural pores.

Fig. 3 shows model results together with experimental data. The calculated parameters are compiled in Table 1. The figure points out the reliable agreement between modelling and experimental data, corresponding to an average absolute relative deviation AARD = 5.9 %, being the higher deviations found for the lower temperature range. The contributions of each individual transport mechanism for H_2 permeation are illustrated in Fig. 7. As may be observed, H_2 permeance takes place mainly by Knudsen diffusion, with a minor contribution from viscous flow. Besides, as expected from the decreasing trend of permeance against temperature, the activated gaseous diffusion is not significant. These results are in total agreement with the previous discussion around Figs. 5 and 6.

The optimized parameter of the activated diffusion $\left(g_{sup}l_d\sqrt{8/\pi\Re}/Z\delta\right)$ of molecules larger than AM-3 pore size, i.e. N_2 and CO_2, is one order of magnitude inferior to that of H_2 and He (1.719×10^{-11} *versus* 2.148×10^{-10}), due to the relative sizes of the molecules and the permeated pores. With respect to the activation energies, the small values found for N_2 and CO_2 (1.7 and 4.0 kJ mol^{-1}, respectively) in relation to those of H_2 and He (13.3 and 11.0 kJ mol^{-1}, respectively) rely upon the average pore diameters where diffusion occurs, namely the inter- and intracrystalline micropores of the AM-3-1 membrane. In particular, $E_{a,g}(H_2) > E_{a,g}(He)$ reflects the same relation between their kinetic diameters, since both molecules prevail on the same type of pores.

As aforementioned, single gas transport across porous membranes occurs essentially by viscous, Knudsen, activated gaseous and surface diffusions. The existence of macro- and meso-defects in porous materials favours the first two mechanisms whereas intracrystalline and structural micropores embrace the remaining ones. In order to model all contributions in new AM-3 membranes, the experimental results reported by Lin et al. [40] for the first AM-3 membrane (denoted by AM-3-2 membrane) will also be analysed in this work. This membrane was synthesized on a tubular stainless-steel support by seeded hydrothermal synthesis (see Ref. [40] for a detailed description).

The experimental data published for the AM-3-2 membrane with pure H_2, N_2, CO_2, and O_2 are given in Fig. 8 and point out it contains not only macro- and meso-defects, but also intercrystalline micropores. In fact, the constant permeances of N_2, CO_2, and O_2 over temperature must rely on the necessary existence

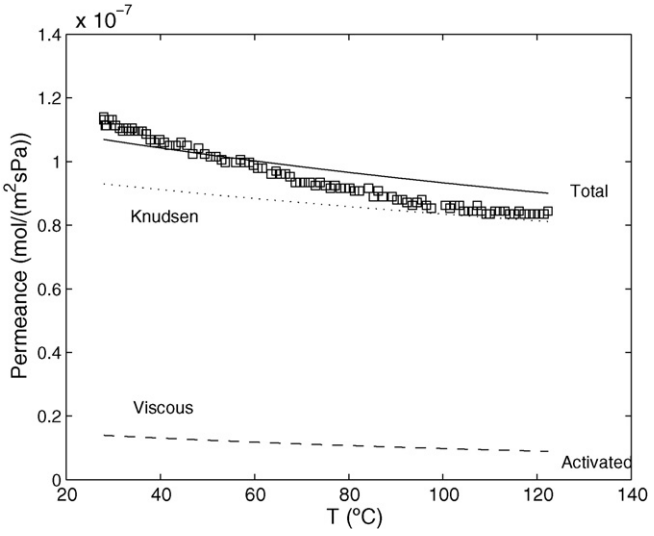

Fig. 7. Contributions of the different transport mechanisms for H_2 permeation through AM-3-1 membrane at $\Delta P = 1$ bar.

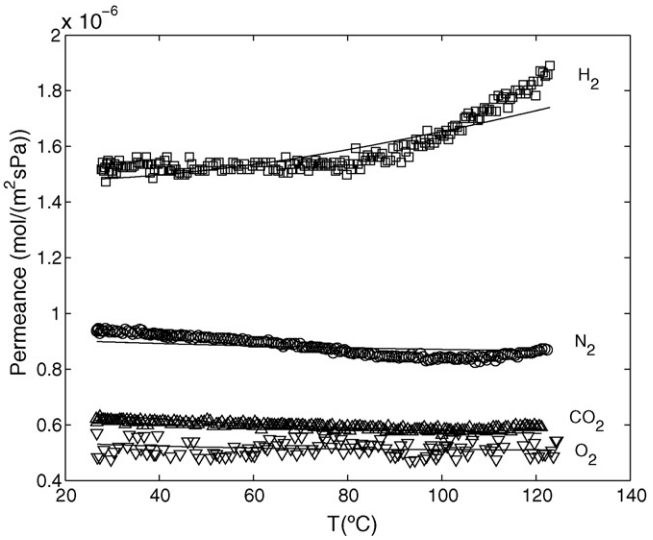

Fig. 8. Calculated and experimental results for permeation of H_2, N_2, O_2, and CO_2 in AM-3-2 membrane for $\Delta P = 0.2$ bar.

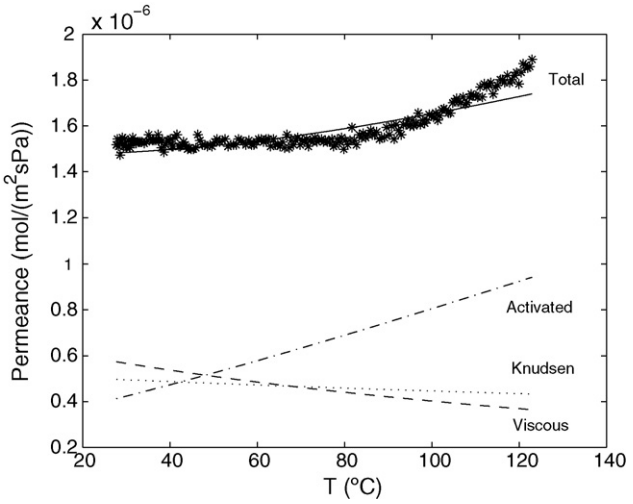

Fig. 9. Contribution of each transport mechanism for the H_2 permeation through AM-3-2 membrane for $\Delta P = 0.2$ bar.

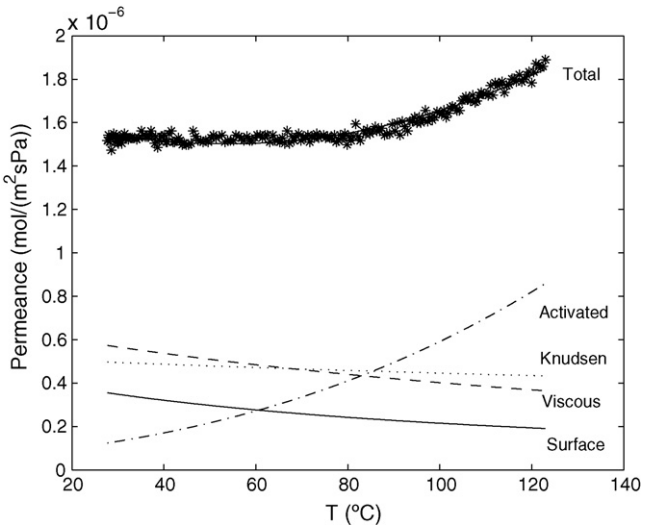

Fig. 10. Contribution of each transport mechanism for the H_2 permeation through AM-3-2 membrane, including surface diffusion, for $\Delta P = 0.2$ bar.

of an activated contribution to compensate the lowering effect of the viscous and Knudsen components. Results revealed the membrane has significant intercrystalline micropores, since N_2, CO_2, and O_2 did permeate the membrane. On the other hand, the hydrogen permeation exhibits the desired exponential behaviour with temperature, since its small diameter superimposes the intracrystalline activated diffusion which overlaps the negative contribution of viscous and Knudsen fluxes: the Π values increase from 1.5×10^{-6} to 1.9×10^{-6} mol m^{-2} s Pa, when temperature varies from ca. 80 to 120 °C. The experimental data were once more modelled based on the transport mechanisms proposed above. Also for this membrane, surface diffusion was not taken into account. Fig. 8 shows the good agreement found between modelling and data points, corresponding to AARD = 2.5 %.

The contribution of each transport mechanism for the H_2 permeation is illustrated in Fig. 9, which evidences identical components of Knudsen and viscous flow to the transport through defects. Besides, the activated gaseous diffusion is considerable, being more important at higher temperatures, as expected. Table 1 compiles the fitted model parameters. Also in this case, the activated diffusion parameter of molecules larger than AM-3 pore size, i.e. N_2, CO_2, and O_2, is one order of magnitude inferior to that of H_2 (4.916×10^{-6} *versus* 1.769×10^{-5}). Moreover, they are significantly higher than those of the membrane synthesized in this work, corroborating the sound contribution of the activated diffusion for the transport through AM-3-2 membrane. This result is also consentaneous with the increasing trend of the $\Pi - T$ curves. Likewise AM-3-1 membrane, the activation energies found for the molecules larger than AM-3 pore size (3.0, 4.6, and 5.5 kJ mol^{-1} for N_2, CO_2, and O_2, respectively) are smaller than that of H_2 (10.0 kJ mol^{-1}), reflecting distinct diffusing pathways.

The results obtained point out a meaningful H_2 transport through AM-3-2 micropores and, accordingly, surface diffusion has been also included in a second modelling step using Eq. (18). For this purpose, the parameters corresponding to the Knudsen and viscous mechanisms listed in Table 1 were fixed, while those for diffusion through micropores were fitted to the H_2 data. Fig. 10 illustrates the calculated results together with the contributions of each mechanism. It is clear that the model performs quite better as confirmed by the smaller deviation obtained (AARD = 1.1 %). Nonetheless, it should be noted that a higher number of parameters was fitted, which also contributes to the enhanced model results. The parameters obtained are listed in Table 2, and show that the activation energy for diffusion is about two times higher than that obtained assuming $\Pi_s = 0 : 21.6$ against 10.0 kJ mol^{-1}. This is an expected result since higher activation energies increase the permeation sensibility on the temperature, and accordingly the expected increase of permeance after approximately 80 °C is more pronounced (see Fig. 10).

The synthesis of similar narrow pore molecular-sieve materials, suitable for small gases separation, has attracted considerable interest. For instance, van den Bergh et al. [42] have recently studied the permeation and separation characteristics of a DDR zeolite membrane (pore aperture of 0.36 nm × 0.44 nm) and obtained permeances of He, H_2, CO_2, and N_2 in the range of $1–10 \times 10^{-8}$ mol m^{-2} s Pa, which decreased monotonically with temperature. This behaviour was attributed to the presence of surface diffusion mechanism. Tomita et al. [43] measured permeances between 10^{-9} and 10^{-7} mol m^{-2} s Pa for pure helium, hydrogen, carbon dioxide, oxygen, and nitrogen at 301 and 373 K on a DDR type zeolite membrane formed on a porous alumina substrate by hydrothermal process. Sebastian et al. [44] synthesized new microporous titanosilicate membranes with an umbite structure (with pore size around 0.3 nm) on asymmetric TiO_2 tubular supports by seeded hydrothermal synthesis and obtained H_2 permeances around 4.6×10^{-9} mol m^{-2} s Pa. Those membranes were able to separate H_2 from N_2 with high selectivity. In addition, Guan et al. [45] obtained permeances of H_2, CO_2, O_2, and N_2 in the range $(0.8–2.5) \times 10^{-8}$ mol m^{-2} s Pa with an ETS-4 membrane (with pore dimensions of 0.37 nm) prepared on a porous α-alumina support tube by hydrothermal reaction. Notwithstanding, good quality AM-3 membranes (with smaller pore diameter) could be expected to exhibit excellent molecular-sieve properties and accordingly to fulfill the small gases separations demands.

Table 2
Model parameters for H_2 diffusion in AM-3-2 membrane, after taking surface diffusion into account (Knudsen and viscous parameters may be found in Table 1).

$g_{sup}\frac{\rho}{\delta}D_s^0K_0$ (kg m^{-3} s^{-2} Pa) Eq. (17)	$g_{sup}\frac{l_d}{Z\delta}\left(\frac{8}{\pi\Re}\right)^{0.5}$ (mol K/J)$^{0.5}$ Eq. (10)	$\Delta H_{ads} - E_{a,s}$ (kJ mol^{-1}) Eq. (17)	$E_{a,g}$ (kJ mol^{-1}) Eq. (10)
2.680×10^{-8}	5.349×10^{-4}	6.465×10^{3}	21.6

5. Conclusions

In this work, a new AM-3 membrane (AM-3-1) has been synthesized and characterized in detail by gas permeation experiments. The results obtained here and those from a previous publication (membrane AM-3-2) were modelled taking into account the various transport mechanisms involved in such microporous titanosilicate: viscous and Knudsen flows through macro and mesodefects, and both activated gaseous and surface diffusions in micropores.

The experimental observations registered for the AM-3-1 membrane with H_2, He, N_2, and CO_2 evidenced that the prevailing transport mechanisms were viscous and Knudsen. The $\Pi - T$ curves were monotonously decreasing, which is typical of both contributions. Furthermore, the Knudsen dominance was verified by the linear trend found between permeances and the inverse of the square root of the molecular weight ($\Pi \propto 1/M^{0.5}$). Concerning the viscous flow contribution, its dependence on gas viscosity implies a subsequent relationship with kinetic diameter and molecular weight, which for Chapman–Enskog type equations writes $\eta \propto M^{0.5}/d_k^2$. The measured permeances roughly followed a direct proportionality to $d_k^2/M^{0.5}$, indicating some contribution from viscous flow, once Π_v is inversely proportional to viscosity. Modelling of experimental $\Pi - T$ curves clearly supported the previous conclusions.

The analysis of the results for AM-3-2 with pure H_2, N_2, CO_2, and O_2 has been included to emphasize the role played by micropores in diffusion. The results reported pointed out it contains also intercrystalline micropores. The hydrogen permeation exhibited the desired exponential behaviour with temperature, since its small diameter superimposes an activated diffusion component, which overlaps the negative contributions of viscous and Knudsen fluxes.

With respect to modelling, the embodied parameters have been fitted to the experimental data. The calculated results are in good agreement with measurements giving rise to absolute average relative deviations between 1.1% and 2.5%. The activation energies found for molecules larger than AM-3 pore size (N_2, CO_2, and O_2) are smaller than that for hydrogen, which reflects different diffusion pathways. In fact, hydrogen permeates also inter and intracrystalline micropores. Moreover, the activation diffusion parameter of N_2, CO_2, and O_2 is one order of magnitude inferior to that of H_2.

Acknowledgments

Patrícia F. Lito, Chun F. Zhou and Ana S. Santiago wish to thank grants provided by Fundação para a Ciência e Tecnologia (Portugal) (SFRH/BD/25580/2005, SFRH/BPD/26690/2006 and SFRH/BPD/48258/2008). The synthesis and characterization work was supported by research projects PTDC/CTM/73643/2006 and PTDC/EQU-EQU/100476/2008 of FCT.

References

[1] J. Caro, M. Noack, P. Kolsch, R. Schafer, Zeolite membranes – state of their development and perspective, Microporous Mesoporous Mater. 38 (2000) 3–24.
[2] J. Rocha, M.W. Anderson, Microporous titanosilicates and other novel mixed octahedral–tetrahedral framework oxides, Eur. J. Inorg. Chem. (2000) 801–818.
[3] Z. Lin, J. Rocha, P. Brandao, A. Ferreira, A.P. Esculcas, J.D.P. deJesus, A. Philippou, M.W. Anderson, Synthesis and structural characterization of microporous umbite, penkvilksite, and other titanosilicates, J. Phys. Chem. B 101 (1997) 7114–7120.
[4] Y.L. Liu, H.B. Du, F.Q. Zhou, W.Q. Pang, Synthesis of a new titanosilicate: an analogue of the mineral penkvilksite, Chem. Commun. (1997) 1467–1468.
[5] Y.L. Liu, H.B. Du, Y.H. Xu, H. Ding, W.Q. Pang, Y. Yue, Synthesis and characterization of a novel microporous titanosilicate with a structure of penkvilksite-1M, Microporous Mesoporous Mater. 28 (1999) 511–517.
[6] Z. Lin, J. Rocha, A. Navajas, C. Tellez, J.Q. Coronas, J. Santamaria, Synthesis and characterisation of titanosilicate ETS-10 membranes, Microporous Mesoporous Mater. 67 (2004) 79–86.
[7] Z. Lin, J.P. Rainho, J. Rocha, L.D. Carlos, Preparation of photoluminescent materials from a lanthanide-doped microporous titanosilicate precursor, Adv. Mater. Forum III 514–516 (Pts 1 and 2) (2006) 123–127.
[8] A.J. Burggraaf, L. Cot, Fundamentals of Inorganic Membranes Science and Technology, Elsevier, Amsterdam, The Netherlands, 1996.
[9] J.R. Xiao, J. Wei, Diffusion mechanism of hydrocarbons in zeolites.1 Theory, Chem. Eng. Sci. 47 (1992) 1123–1141.
[10] A.J. Burggraaf, Single gas permeation of thin zeolite (MFI) membranes: theory and analysis of experimental observations, J. Membr. Sci. 155 (1999) 45–65.
[11] R.J.R. Uhlhorn, K. Keizer, A.J. Burggraaf, Gas-transport and separation with ceramic membranes.1. Multilayer diffusion and capillary condensation, J. Membr. Sci. 66 (1992) 259–269.
[12] E.R. Gilliland, R.F. Baddour, G.p. Perkinso, K.J. Sladek, Diffusion on surfaces.1. Effect of concentration on diffusivity of physically adsorbed gases, Ind. Eng. Chem. Fund. 13 (1974) 95–100.
[13] R. Krishna, Problems and pitfalls in the use of the Fick formulation for intraparticle diffusion, Chem. Eng. Sci. 48 (1993) 845–861.
[14] M. Okazaki, H. Tamon, R. Toel, Interpretation of surface flow phenomenon of adsorbed gases by hopping model, AIChE J. 27 (1981) 262–270.
[15] E.R. Gilliland, R.F. Baddour, J.L. Russell, Rates of flow through microporous solids, AIChE J. 4 (1958) 90–96.
[16] W.J.W. Bakker, L.J.P. vandenBroeke, F. Kapteijn, J.A. Moulijn, Temperature dependence of one-component permeation through a silicalite-1 membrane, AIChE J. 43 (1997) 2203–2214.
[17] J.R. Xiao, J. Wei, Diffusion mechanism of hydrocarbons in zeolites.2. Analysis of experimental-observations, Chem. Eng. Sci. 47 (1992) 1143–1159.
[18] R. Krishna, Multicomponent surface-diffusion of adsorbed species – A description based on the generalized Maxwell–Stefan equations, Chem. Eng. Sci. 45 (1990) 1779–1791.
[19] R. Krishna, R. Baur, Modelling issues in zeolite based separation processes, Sep. Purif. Technol. 33 (2003) 213–254.
[20] R. Krishna, D. Paschek, Separation of hydrocarbon mixtures using zeolite membranes: a modelling approach combining molecular simulations with the Maxwell–Stefan theory, Sep. Purif. Technol. 21 (2000) 111–136.
[21] R. Krishna, D. Paschek, R. Baur, Modeling the occupancy dependence of diffusivities in zeolites, Microporous Mesoporous Mater. 76 (2004) 233–246.
[22] P.F. Lito, A.S. Santiago, S.P. Cardoso, B.R. Figueiredo, C.M. Silva, New expressions for single and binary permeation through zeolite membranes for different isotherm models, J. Memb. Sci., submitted for publication.
[23] J. Romero, C. Gijiu, J. Sanchez, G.M. Rios, Unified approach of gas, liquid and supercritical solvent transport through microporous membranes, Chem. Eng. Sci. 59 (2004) 1569–1576.
[24] W.J.W. Bakker, F. Kapteijn, J. Poppe, J.A. Moulijn, Permeation characteristics of a metal-supported silicalite-1 zeolite membrane, J. Membr. Sci. 117 (1996) 57–78.
[25] M. Knudsen, Die gesetze der molekularströmung und der inneren reibungsströmung der gase durch röhren, Annalen der Physik (Leipzig) 28 (1909) 75–130.
[26] A. Fick, On liquid diffusion, Philos. Mag. Series 4 10 (1855) 30–39.
[27] A. Fick, Uber diffusion, Poggendorff's Annalen der Physik und Chemie 94 (1855) 59–86.
[28] D.M. Ruthven, Principles of adsorption and adsorption processes, Wiley, New York, 1984.
[29] R. Krishna, J.A. Wesselingh, Review article number 50 – The Maxwell–Stefan approach to mass transfer, Chem. Eng. Sci. 52 (1997) 861–911.
[30] J.H. Dong, Y.S. Lin, W. Liu, Multicomponent hydrogen/hydrocarbon separation by MFI-type zeolite membranes, AIChE J. 46 (2000) 1957–1966.
[31] T.Q. Gardner, A.I. Flores, R.D. Noble, J.L. Falconer, Transient measurements of adsorption and diffusion in H-ZSM-5 membranes, AIChE J. 48 (2002) 1155–1167.
[32] J. Zah, H.M. Krieg, J.C. Breytenbach, Single gas permeation through compositionally different zeolite NaA membranes: observations on the intercrystalline porosity in an unconventional, semicrystalline layer, J. Membr. Sci. 287 (2007) 300–310.
[33] W.D. Zhu, P. Hrabanek, L. Gora, F. Kapteijn, J.A. Moulijn, Role of adsorption in the permeation of CH_4 and CO_2 through a silicalite-1 membrane, Ind. Eng. Chem. Res. 45 (2006) 767–776.
[34] L.J.P. van den Broeke, W.J.W. Bakker, F. Kapteijn, J.A. Moulijn, Transport and separation properties of a silicalite-1 membrane – I. Operating conditions, Chem. Eng. Sci. 54 (1999) 245–258.
[35] G.R. Gavalas, Diffusion in microporous membranes: measurements and modeling, Ind. Eng. Chem. Res. 47 (2008) 5797–5811.
[36] J.M. van de Graaf, M.F. Kapteijn, J.A. Moulijn, Methodological and operational aspects of permeation measurements on silicalite-1 membranes, J. Membr. Sci. 144 (1998) 87–104.
[37] J. Coronas, J.L. Falconer, R.D. Noble, Characterization and permeation properties of ZSM-5 tubular membranes, AIChE J. 43 (1997) 1797–1812.
[38] A.J. Burggraaf, Z.A.E.P. Vroon, K. Keizer, H. Verweij, Permeation of single gases in thin zeolite MFI membranes, J. Membr. Sci. 144 (1998) 77–86.
[39] N. Nishiyama, L. Gora, V. Teplyakov, F. Kapteijn, J.A. Moulijn, Evaluation of reproducible high flux silicalite-1 membranes: gas permeation and separation characterization, Sep. Purif. Technol. 22–23 (2001) 295–307.

[40] Lin Z., Zhou C.F., Lito P.F., Santiago A.S., Rocha J., Silva C.M., Lin Z., Synthesis and characterization of a new microporous titanosilicate AM-3 membrane, Microporous Mesoporous Mater., submitted for publication.
[41] T.H. Chung, L.L. Lee, K.E. Starling, Applications of kinetic gas theories and multiparameter correlation for prediction of dilute gas viscosity and thermal-conductivity, Ind. Eng. Chem. Fund. 23 (1984) 8–13.
[42] J. van den Bergh, A. Tihaya, F. Kapteijn, High temperature permeation and separation characteristics of an all-silica DDR zeolite membrane, Microporous Mesoporous Mater. 132 (2010) 137–147.
[43] T. Tomita, K. Nakayama, H. Sakai, Gas separation characteristics of DDR type zeolite membrane, Microporous Mesoporous Mater. 68 (2004) 71–75.
[44] V. Sebastian, Z. Lin, J. Rocha, C. Tellez, J. Santamaria, J. Coronas, Improved Ti-silicate umbite membranes for the separation of H_2, J. Membr. Sci. 323 (2008) 207–212.
[45] G.Q. Guan, K. Kusakabe, S. Morooka, Separation of nitrogen from oxygen using a titanosilicate membrane prepared on a porous α-alumina support tube, Sep. Sci. Technol. 37 (2002) 1031–1039.